Tectonophysics 611 (2014) 83–93

Contents lists available at ScienceDirect

Tectonophysics

journal homepage: www.elsevier.com/locate/tecto

New free-air and Bouguer gravity fields of Taiwan from multiple platforms and sensors

Cheinway Hwang [a,*], Hung-Jui Hsu [a], Emmy T.Y. Chang [b], W.E. Featherstone [c], Robert Tenzer [d], Tzuyi Lien [a], Yu-Shen Hsiao [e], Hsuan-Chang Shih [f], Pang-Ho Jai [a]

[a] Department of Civil Engineering, National Chiao Tung University, 1001 Ta Hsueh Road, Hsinchu, Taiwan
[b] Institute of Oceanography, National Taiwan University, No. 1, Sec. 4, Roosevelt Road, Taipei 106, Taiwan
[c] Western Australian Centre for Geodesy & The Institute for Geoscience Research, Curtin University of Technology, GPO Box U1987, Perth, WA 6845, Australia
[d] Institute of Geodesy and Geophysics, School of Geodesy and Geomatics, Wuhan University, 129 Luoyu Road, Wuhan, China
[e] Department of Soil and Water Conservation, National Chung Hsing University, 250 Kuo Kuang Rd., Taichung 402, Taiwan
[f] Research Center for Environmental Changes, Academia Sinica, 128 Academia Road, Section 2, Nankang, Taipei 115, Taiwan

ARTICLE INFO

Article history:
Received 19 August 2013
Received in revised form 7 November 2013
Accepted 16 November 2013
Available online 27 November 2013

Keywords:
GPS
Gravity anomaly
Gravity network adjustment
Least-squares collocation
Taiwan

ABSTRACT

We construct 1′ × 1′ grids of free-air and Bouguer gravity anomalies around Taiwan with well-defined error estimates for quality assessment. The grids are compiled from land, airborne and shipborne gravity measurements, augmented with altimeter gravity at sea. Three sets of relative land gravity measurements are network-adjusted and outlier-edited, yielding accuracies of 0.03–0.09 mGal. Three airborne gravity sets are collected at altitudes 5156 and 1620 m with accuracies of 2.57–2.79 mGal. Seven offshore shipborne gravity campaigns around Taiwan and its offshore islands yield shallow-water gravity values with 0.88–2.35 mGal accuracies. All data points are registered with GPS-derived geodetic coordinates at cm–dm accuracies, allowing for precise gravity reductions and computing gravity disturbances. The various datasets are combined by the band-limited least-squares collocation in a one-step procedure. In the eastern mountainous (or offshore) region, Bouguer anomalies and density contrasts without considering the oceanic (or land) topographic contribution are underestimated. The new grids show unprecedented tectonic features that can revise earlier results, and can be used in a broad range of applications.

1. Introduction

Taiwan is situated at the convergent tectonic plate boundary of the Eurasian and Philippine Plates. The collision of the two plates results in a rough topography and complex geological and tectonic setup, and consequently large spatial gravity variations. For example, large mass deficiency, consequently large negative free-air gravity anomalies (FAs), occurs in the trenches east of Taiwan as a result of subduction that moves masses deep into the mantle. The high mountain ranges of Taiwan are packed with surplus masses that are mainly a result of tectonic plate collision, leading to gravity highs positively correlated with the topography. In the western coastal plains, the Fas are largely negative due to low-density sedimentary deposits filled in the foreland depression. East of Taiwan, large, seamount-typed gravity highs occur around volcano islets such as Ludao and Lanyu off the southeast coast of Taiwan and Ryukyu Islands. Such gravity signatures have been reported in several publications addressing gravity observations and processing around Taiwan, among them are Yen et al. (1990), Hsu et al. (1998) and Hwang et al. (2007). The rich gravity signature of Taiwan, originating from both surface and deep processes, has attracted many domestic and international scientists to study phenomena ranging from geodynamics to oceanography. Sample subjects of study using Taiwan's existing gravity data are Moho depth modeling (Hsieh et al., 2010; Kuo-Chen et al., 2012), estimation of effective elastic thickness (Lin and Watts, 2002), joint inversion of Taiwan density structure (Masson et al., 2012) and altimeter study of Kuroshio Current (Hwang and Kao, 2002). We expect that reliable and densely covered gravity values, particularly in the high mountains of Taiwan, can revise the current results.

The earliest gravity map of Taiwan since the World War II was published by the Chinese Petroleum Corporation in search of oil fields in western Taiwan (Chang and Hu, 1981; Hsieh and Hu, 1972). In an effort to understand the tectonic structure of Taiwan, the Institute of Earth Science (IES), Academia Sinica, collected point gravity values in Taiwan over 1980–1987, spaced at an mean distance of 7 km. One notable result of this effort is gravity measurements at some extreme summits of Taiwan, where currently no other source of gravity data exists. Despite the huge popularity of this gravity dataset, no document exists that shows whether the relative gravity measurements associated

* Corresponding author at: Dept of Civil Engineering, National Chiao Tung University, 1001 Ta Hsueh Road, Hsinchu 300, Taiwan.
E-mail addresses: cheinway@mail.nctu.edu.tw, cheinway@gmail.com (C. Hwang), W.Featherstone@curtin.edu.au (W.E. Featherstone).

0040-1951/$ – see front matter © 2013 Elsevier B.V. All rights reserved.
http://dx.doi.org/10.1016/j.tecto.2013.11.027

with the gravity values were rigorously network-adjusted (Hwang et al., 2002; Torge, 1989) and there are no error estimates associated with the point gravity values.

Since 2000, several projects of various purposes in Taiwan have been funded to collect gravity data. Except for the three airborne gravity surveys that have been documented in journal papers (e.g., Hwang et al., 2007, 2012), most of these gravity datasets are only documented in reports in Chinese not available to the scientific community. Highlights of such gravity datasets are listed below. The gravity data were collected in multiple platforms and multiple sensors ranging from moving to static platforms, and by multiple measurement styles, ranging from the along-track style to the network-wise style (Torge, 1989). The gravity values were registered with precise positions (geodetic latitude and longitude and geometric height) by GPS, allowing for precise computations of terrain effect and gravity disturbance; the latter is important for geoid modeling (Featherstone, 2013; Kirby, 2003) and Moho depth modeling (Tenzer et al., 2009). Many land gravity measurements were collected over high mountains that are difficult to access. For the first time, offshore gravity values at few tens of m to the coasts of Taiwan and its offshore islands were collected by small ships, with the ship positioning accuracies by GPS reaching few cm. However, these various gravity datasets have not been optimally edited and combined.

The objective of this paper is to collect, compile and edit gravity data from the aforementioned gravity projects to produce a high precision, high resolution and coherent gravity dataset of Taiwan, complete with standard errors of the point and gridded gravity values (Section 2). Because Bouguer gravity anomalies (BAs) are increasingly important in tectonic structure studies and in the joint gravity-seismic inversion of density contrast, we will investigate several scenarios of BA computations considering the topographic contributions from land and ocean (Section 3). Confronted with different spatial resolutions and accuracies in the original datasets, we will use a frequency-based method to combine such datasets to form optimal FA and BA grids (Section 4). New tectonic features based on the new gravity field will be highlighted (Section 5). We expect that the outcome from this paper will benefit geodetic studies using Taiwan gravity data, and projects such as TAIGER (Huang et al., 2012; Kuo-Chen et al., 2012), which are dedicated to testing the models of Taiwan orogeny.

2. Gravity datasets and processing

2.1. Land gravity data collected in a network mode

Figs. 1 and 2 show the distribution of all gravity measurements collected in this paper. The land gravity measurements were collected over 2000–2012 using relative gravimeters based on a network-like observation scheme (Hwang et al., 2002; Torge, 1989), allowing for a network adjustment to remove data outliers and to estimate the standard errors of the gravity values (see below). Table 1 lists the key statistics associated with the gravity values. All coordinates associated with the gravity values were determined by GPS, allowing for determining gravity disturbances and for reliable reductions of BAs. The GPS positioning sessions last between 0.5 and 1 h, yielding positioning accuracies at few cm level for gravity sites. The All-terrain set represents the most important dataset collected over 2000–2006 and the data are distributed over all types of terrain in Taiwan, with a mean point spacing of 3 km. There are three subsets in All-terrain. The first two subsets contain gravity values spaced at 1–2 km on the first-order benchmarks in Taiwan, and on offshore islands Kinmen (KM), Matzu (MZ), Ludao (LD), Lanyu (LY), Penghu (PH) and Siaoliouciou (SL), with cm-level GPS coordinates and mm-level orthometric heights (in the vertical datum of Taiwan). The data in Mountain-1 were collected over 2011–2012 and are distributed over high mountains of northern Taiwan and the Coastal Range (CoR) of eastern Taiwan.

As an example, here we show the effort of the network adjustment for the relative gravity measurements collected in the campaign of 2004–2006 (the third subset in All-terrain). The adjustment treated 14,891 relative gravity measurements and constrained (fixed) the gravity values at 11 sites determined by two FG5 absolute gravimeters (with 1 μGal accuracy). With the tau-test method of outlier detection (Pope, 1976), a total of 67 outliers were detected and removed in several rounds of iteration. The final round of adjustment yielded 4399 adjusted gravity values. The standard errors of the adjusted gravity values range from 0.00 (at the absolute gravity stations, not included in the statistics in Table 1) to 0.09 mGal. The residuals of observations range from −0.18 to 0.19 mGal, and the a posteriori standard error of unit weight is 0.049 mGal, which is about the mean accuracy achieved

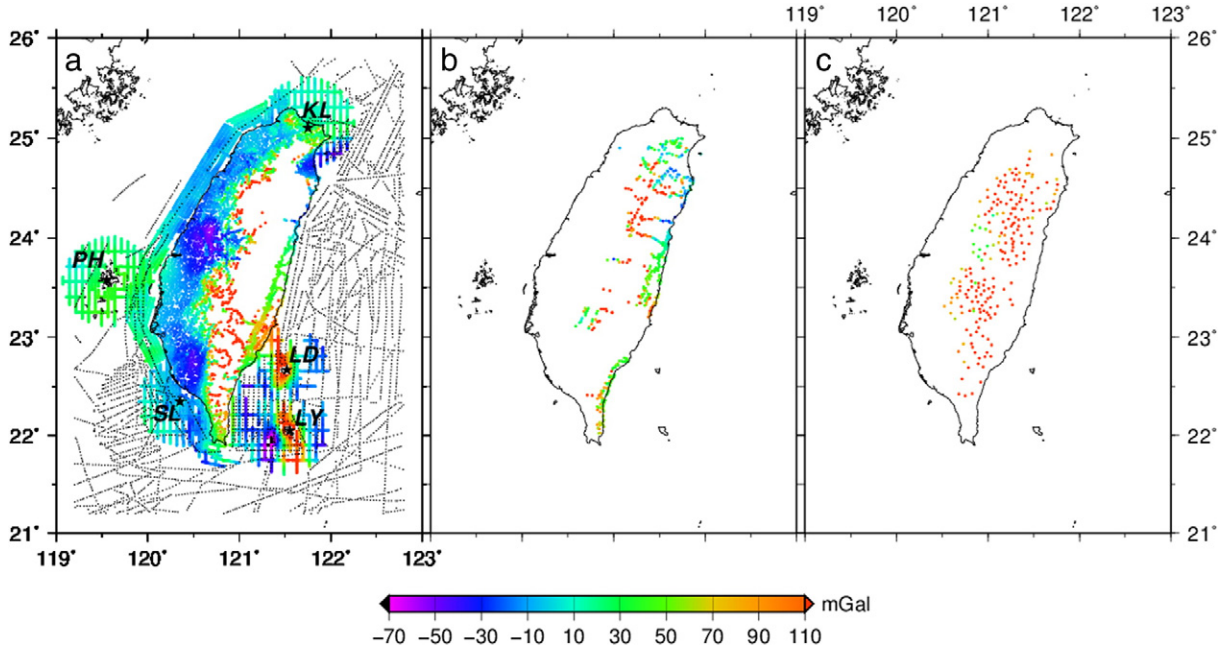

Fig. 1. (a) Point free-air gravity anomalies at ground level and sea level (from All-terrain in Table 1 and offshore surveys), black dots in oceans show gravity data from Hsu et al. (1998), stars show the tide gauge stations at Keelung and offshore islands, (b) point free-air gravity anomalies collected during 2011–2012 (Mountain-1 in Table 1), (c) point free-air gravity anomalies collected during 1980–1987 (Mountain-2 in Table 1).

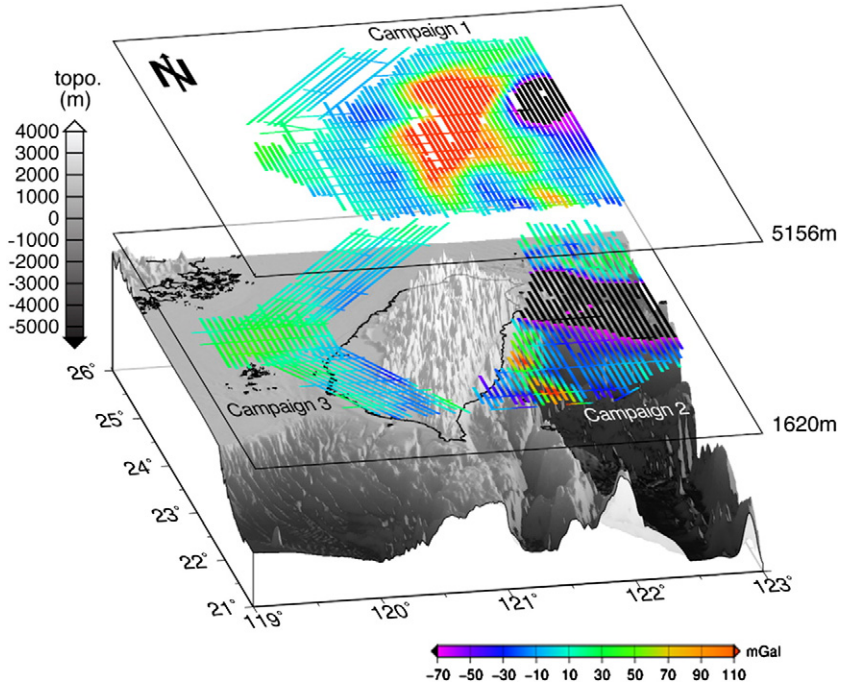

Fig. 2. Point free-air gravity anomalies at flight levels from three airborne gravity campaigns.

by the relative gravimeters in the surveys. A cross validation (cf. Sproule et al., 2006) of the GPS-determined elevations associated with the 4399 point gravity values was made against the latest 3″ × 3″ digital elevation model (DEM) of Taiwan, yielding 51 erroneous elevations (Fig. 3a). The 3″ × 3″ DEM was constructed from elevation data from the Aerial Survey Office of the Forest Bureau, Taiwan (Hwang et al., 2003). Aided by the 3″ × 3″ DEM and existing gravity data, we confirm that the erroneous elevations are caused by errors in GPS data and site locations. Fig. 3b shows the histogram of the differences between the GPS and DEM-defined elevations, which roughly follow the normal distribution. Such erroneous elevations were replaced by the interpolated elevations from the 3″ × 3″DEM for subsequent processing.

Despite our efforts of land gravity data collection over 2000–2012, there are still void zones in some mountainous areas of Taiwan. Therefore, for the final combined grids (Section 4) we also include 281 point gravity values from Yen et al. (1990) at the summits not covered by the All-terrain and Mountain-1 sets. This set is named Mountain-2 in Table 1. These gravity values are at elevations >1000 m and are indispensable. Because the 281 point values contain only latitude, longitude and FAs (at sea level) without gravity error estimates, we made the following updates for this dataset: (1) change the original coordinates to the TWD1997 coordinates using the transformation parameters published by the Ministry of the Interior of Taiwan (Yang et al., 2001), (2) assign elevations to the point data using the latest 3″ × 3″ digital elevation model (the 3″ × 3″DEM is in both the geometric height and orthometric height systems), and (3) assume gravity error of 1 mGal (for combination using the band-limited least-squares collocation, Section 4). The TWD1997 coordinate system is tied to the International Terrestrial Reference Frame and is the official coordinate frame for geodetic control in Taiwan (Yang et al., 2001). The coordinates of the point values of Yen et al. (1990) are in the 1967 geodetic system of Taiwan (TWD67), which has an average horizontal shift of 853 m with respect to TWD1997. With the updates, the 281 point data are consistent with the point data (2000–2012) collected in this paper.

Table 1
Key statistics of the new gravity datasets in Taiwan.

Set	Time	Gravimeter	No. of points	Std. err.[a] (mGal)	Resolution (km)
All-terrain	2000–2006	EG[b]/CG-5	6468	0.04–0.09	Point
Mountain-1	2011–2012	EG	661	0.03–0.04	Point
Mountain-2	1980–1987	LCR-G	281	N/A	Point
Airborne	2004–2009	S-130	388,570	2.57–2.79	4–6
Offshore-1	2006–2010	S-130/ZLS	1,385,731	0.88–1.94	0.5
Offshore-2	2011–2012	S-130/ZLS	633,236	1.33–2.35	0.5

[a] Mean standard error of mobile gravity = RMS crossover difference divided by √2; Standard error of land gravity is from network adjustment.
[b] GRAVITON-EG and Scintrex CG-5.

2.2. Airborne gravity data at multiple altitudes

From 2004 to 2009, three airborne gravity surveys (Fig. 2) were made in Taiwan. The three airborne gravity surveys were carried out over the altitude of 5156 m (one survey) and the altitudes of 1620 m (two surveys). The resulting gravity datasets allow for seeing the gravity signatures from a common source at different wavelengths (heights). The first survey was made at an altitude of 5156 m, covering the area from the central Taiwan Strait to few tens of km off the east coast of Taiwan (Hwang et al., 2007). The other two surveys were made at an altitude of 1620 m, one over the western half of the Taiwan Strait and the islands of Penghu, and another over the Kuroshio Current east of Taiwan, the latter extending to longitude 123° E (Hwang et al., 2012). A coherence analysis shows that the resolving wavelengths of the three gravity datasets range from 4 to 6 km. The 5156-m airborne gravity is particularly important for filling data gaps in high mountains because of its even coverage over the entire Taiwan, with an average line-to-line spacing of 4 km. For example, Fig. 1 shows only few ground data in the eastern half of Central Range (CeR) and in the inaccessible area of Hsuehshan Range (HR). Over the gaps of ground data like these spots, the 5156-m airborne gravity survey provides indispensable gravity information.

In the three airborne surveys, the aircraft positions were determined by GPS using a network of kinematic baselines that optimize the positioning result based on optimal weights for the individual baselines. Using overlapping trajectory analyses, we found that the overall GPS

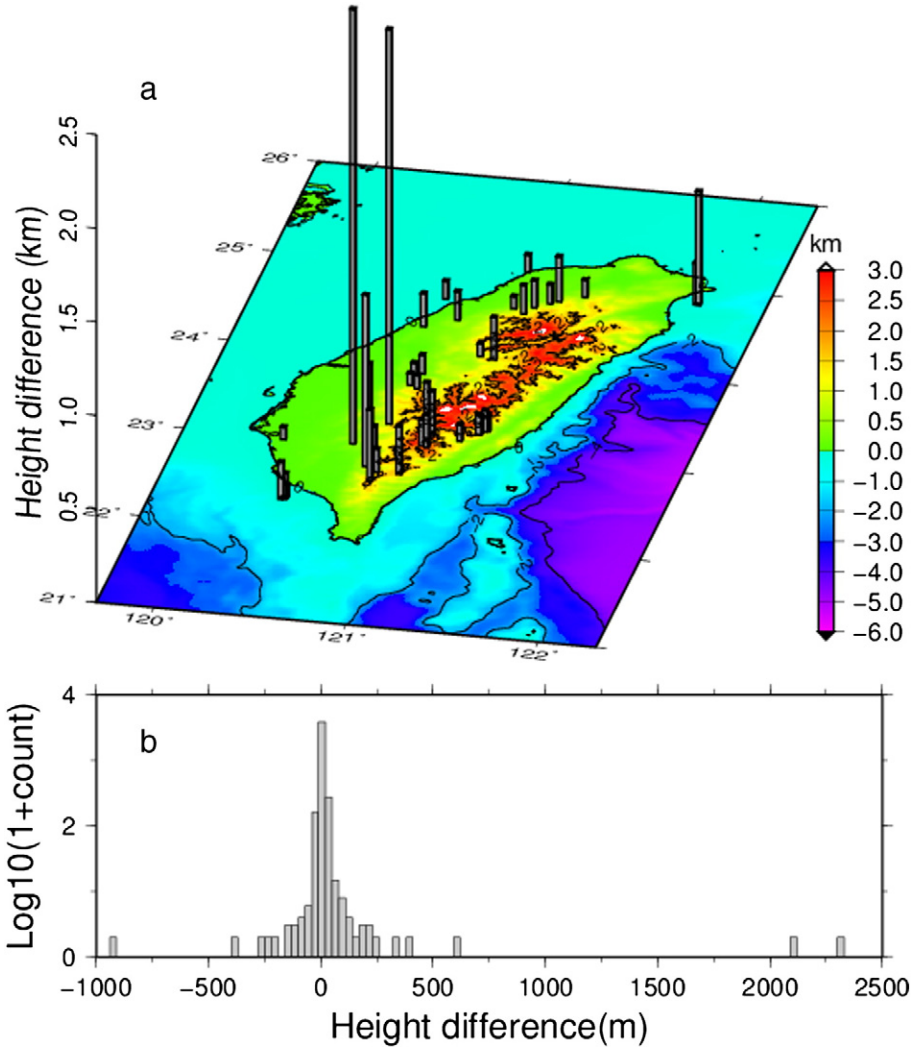

Fig. 3. (a) Locations with large elevation differences between GPS-derived and leveling heights, (b) histogram of the elevation differences.

positioning accuracy is at the dm level, with the velocity error at the mm/s level. With the Gaussian filtering with a 120-s time width, the smoothed velocities and accelerations are sufficient for a sub-mGal correction of the Eötvös effect and vertical accelerations of the aircrafts. The downward continuation of the three sets of airborne gravity data and merging with the ground data turn out to be difficult and will be described in Section 4.

2.3. Offshore shipborne gravity

Two sets of shipborne gravity are listed in Table 1. Offshore-1 contains five campaigns with the gravity values collected around the four offshore islands of Taiwan (LD, LY, PH and SL) and around the Keelung (KL) tide gauge station, in a project to determine the vertical datum offsets between Keelung (the vertical datum of Taiwan island) and these offshore islands. For each offshore island (including Keelung), shipborne gravity readings were collected on a 15-ton fishing boat in a circular area (radius: 50 km) centered at the main tide gauge (Fig. 1). From 2011 to 2012, another two campaigns (Offshore-2) were launched to collect ship gravity values within 20 km offshore Taiwan aiming to improve the coastal geoid accuracy, and the statistics of the two campaigns are listed in Table 1. In the Offshore-2 set, the gravimeters used were S-130 and Zero-length spring (ZLS) ship gravimeters operating at one-Hertz sampling interval. To maximize the ship gravity accuracy, we attended to all details in the gravity surveys, including careful measurement of the gravity value of the tie point at the hosting harbor, careful base reading before departing and after returning from the fieldwork, and detecting problems in gravimeter and GPS readings while the ship was in motion. Unlike a regular campaign in an academic fleet, where gravity survey may play a minor role, whereas in our shipborne gravity survey fieldwork, we regarded correct gravity readings and precise GPS positioning as the two most important points in the shipborne surveys. If the gravity or GPS data along a survey line are in doubt, gravity survey on the line is repeated.

Like the airborne gravity survey, the positioning of the ship was made using GPS relative positioning based on phase observables. For each cruise, a base GPS station was set up at the disembarking harbor of the ship to ensure shortest baselines for optimal kinematic positioning. Crossover analyses of GPS-derived sea surface heights (after ocean tide corrections) suggest that the three-dimensional ship-positioning accuracies range from several cm to dm, depending on the baseline length and the sea status. In few cases, the positioning error can be more than 1 m. Gravity values associated with large positioning errors were excluded. To reduce high-frequency noises caused by the ship dynamics, a Gaussian filter with widths varying from 120 to 150 s was applied to the raw gravity measurements, resulting in about 0.5 km in the spatial resolution (Table 1). The drifts of the along-track data were removed by a crossover adjustment method similar to the one used

for the airborne gravity data. Raw measurements collected at ship turning points and at places with large sea dynamics were excluded. Crossover analyses of the ship data show RMS crossover differences ranging from 0.88 (Penghu) to 2.35 mGal (southwestern Taiwan). This mGal-level gravity accuracy is consistent with that of shipborne gravity collected by gravity-dedicated industry cruise for mineral explorations, and is significantly smaller than that of shipborne gravity collected in large research vessels, which can exceed 10 mGal around Taiwan (Hsu et al., 1998). In addition to the ship data collected in this paper, we also augmented the ship data over the deep waters off Taiwan (not listed in Table 1, but plotted in Fig. 1). Hsu et al. (1998) show that, earlier shipborne data around Taiwan contain large crossover differences (RMS crossover is about 11.2 mGal). Therefore, we used only the shipborne data collected by R/VI' Atalante KSS30 (about 4000 points, with GPS coordinates), whose mean crossover difference is about 2.60 mGal and is close to the accuracy associated with the offshore shipborne gravity in this paper (Table 1). A bias and tilt correction for the R/VI' Atalante KSS30 gravity values with respect to altimeter-derived gravity was made using the method of Hwang and Parsons (1995).

2.4. Altimeter-derived gravity

To enhance the marine gravity around Taiwan, the combined gravity field (Section 4) also uses gravity anomalies derived from re-tracked Geosat/GM, re-tracked ERS-1/GM, repeat Geosat/ERM, ERS-1/35d, ERS-2/35d and TOPEX/Poseidon altimeter data. We experimented with different re-trackers to improve altimeter range measurements, and we find that the sub-waveform threshold retracker (Yang et al., 2011) with a 0.2 threshold value performs the best. The inverse Vening Meinesz formula (Hwang, 1998) was used to compute gravity anomalies from along-track residual sea surface height (SSH) gradients in a remove–compute–restore procedure, with EGM2008 (Pavlis et al., 2013) to degree 2190 as the reference field. The result is the NCTU12 field. In Table 2, we compare the gravity values from NCTU12 and two other altimeter-derived gravity grids, Sandwell V18.1 (Sandwell and Smith, 2009) and DTU10 (Andersen, 2010), with our offshore shipborne gravity values (Section 2.4). All fields perform quite similarly, but NCTU12 performs the best. The NCTU12 gravity field was later merged with the in situ gravity in Section 4.

3. Computation of point Bouguer anomalies on land and sea

For the reason of the optimal downward continuation and optimal combination given in Section 4, we first computed point BAs at the gravity stations in Fig. 1. We computed the topographic gravity effect using the one-step method (Hwang et al., 2007):

$$A_T\left(x_p,y_p,h_p\right)=G\int_x\int_y\rho(x,y)K(x,y,h)dxdy=G\int_x\int_y\rho(x,y)\left[\frac{1}{\sqrt{\left(x-x_p\right)^2+\left(y-y_p\right)^2+\left(h-h_p\right)^2}}-\frac{1}{\sqrt{\left(x-x_p\right)^2+\left(y-y_p\right)^2+{h_p}^2}}\right]dxdy \tag{1}$$

where G is the gravitational constant and ρ is the density, (x_p, y_p, h_p) are the coordinates (horizontal and vertical components) of the computation point and (x, y, h) are the coordinates of the contributing point. As shown in Fig. 4, the topographic effect includes both the contributions from the mass above the geoid on land and the crust-ocean mass difference below mean sea level (MSL) at sea. Here we assume the geoid on land is the extension of MSL. The elevations of the land gravity stations (i.e., h_1, Fig. 4, at P1) used for the numerical integration are the orthometric heights from leveling or from GPS geometric heights minus the Taiwan geoid model (Hwang et al., 2013). The elevations for the marine gravity data are set to zero (i.e. h_s, Fig. 4, at P2). For airborne gravity data, the elevations are the flight altitudes (i.e. h_a, Fig. 4, at P3). In Eq. (1), the density is set to 2.67 g/cm^3 for land, and 1.64 g/cm^3 for sea. In addition, the elevation of a contributing point in Eq. (1) is positive on land (i.e. h_i^{Land}, Fig. 4), but negative at sea (i.e. h_i^{ocean}, Fig. 4). The BA is the difference between FA and the topographic gravity effect:

$$\Delta g_B=\Delta g_F-A_T \tag{2}$$

where Δg_F is the FA (Figs. 1 and 2). For a land gravity station, the integration kernel $K(x, y, h)$ is negative for an oceanic contributing point, and is non-negative or negative ($0 \le h \le 2h_p$ or $h > 2h_p$) for a land contributing point. This implies that, if we neglect the oceanic topographic effect, the resulting BAs on land in Eq. (2) will be smaller than the BAs that consider both the land and oceanic contributions. Likewise, for an oceanic gravity station, if we consider only the oceanic contribution without considering the land contribution, the BA will be also underestimated (see the example below).

We used combined DEMs for BA computations in this paper. First, the gridded elevations were converted to point elevations containing latitudes, longitudes and elevations. On land, the point elevations were generated from the 3″ × 3″ DEM (Hwang et al., 2003). At sea, the point elevations were generated from the 1′ × 1′ ETOPO1 (Amante and Eakins, 2009). We then used the tensioned-spline method of GMT (Wessel and Smith, 1998) to form a combined 3″ × 3″ DEM grid, which was re-sampled to form a 9″ × 9″ grid. The 3″ × 3″ and 9″ × 9″ DEM grids are for computing the inner zone and outer zone effects using the Gaussian quadrature integration for Eq. (1). The radii for the inner zone and outer zone effects are set to 20 and 200 km, based on the result of Hwang et al. (2007).

Following the discussion related to Eq. (2), we investigated the topographic gravity effects in BA with the following two cases: (1) considering both land and oceanic contributions for all gravity stations, and (2) considering land contribution only for land gravity stations and oceanic contribution only for oceanic gravity stations. The computation in Case 1 is regarded as the most rigorous (and theoretically correct) one. For this investigation, the land gravity (Table 1) and altimeter-derived gravity data (Section 2.4) were used. Fig. 5 shows the differences in BA from Cases 1 and 2 (Case 2 BA minus Case 1 BA). For the BA differences on land, there are large differences of up to ~10 mGal occurring over the eastern mountainous area of Taiwan, due to the large ocean depths and oceanic contribution neglected in Eq. (1) over the Pacific Ocean east of Taiwan. There are also differences of up to ~5 mGal over the eastern offshore area of Taiwan when computing the BAs at sea with the land contribution neglected. Fig. 5 shows that BA difference increases with the elevation of gravity station. The BA differences (in absolute values) along the Longitudinal Valley (LV) are smaller than the differences in the CeR and the CoR (Fig. 5). The BA differences decrease westwards, becoming zero near the shores in the western coastal area of Taiwan. Again, the negative BA differences imply that, if we consider the land contribution only for a land station, or the oceanic contribution only for an oceanic station (Case 2), the resulting BAs are underestimated and the density contrasts are underestimated. In conclusion, for an area

Table 2
Statistics of differences (in mGal) between offshore shipborne gravity anomalies and values from three altimeter-derived fields.

Field	Max	Min	Mean	STD	RMS
NCTU12	47.758	−39.929	0.213	8.470	8.472
Sandwell V18.1	49.410	−43.415	−0.202	8.685	8.687
DTU10	48.875	−42.377	−0.126	8.512	8.512

with complex terrain and bathymetry like Taiwan, we should consider the contributions from both land and ocean when computing BAs for land and oceanic stations. This conclusion also applies to the BAs associated with the airborne gravity data.

4. Gravity downward continuation and combination by band-limited least squares collocation

With the different spatial resolutions, accuracies and altitudes of the gravity datasets, combining them to form gravity grids for subsequent analyses is challenging. The airborne and shipborne gravity data are filtered, so such data are band-limited and can only contribute gravity signals at certain wavelengths (Novák and Heck, 2002). The land gravity data are point-wise data and hence contain full signals, plus random errors. The combination must lead to an optimal gravity field that preserves the major features from the original contributions. In this paper, the combined FA and BAs are defined at sea level, so downward continuations of the three airborne gravity datasets were necessary. Several methods have been attempted to combine the various datasets, and the following recipe is found to produce the optimal result, based on the comparison of the final BAs with the geological units of Taiwan, and an inter-comparison between the ground-only and airborne only BAs (see below). A direct combination of the various sources of FAs produces large gravity artifacts. In the mountainous area, a direct downward continuation of FA will require a heavy filter that downplays significantly the contribution of the 5156-m airborne gravity dataset.

In our final recipe of data combination, the first step was to strip both the gravity effects of the topography above the geoid and bathymetry below the MSL from all gravity values to produce point gravity BAs

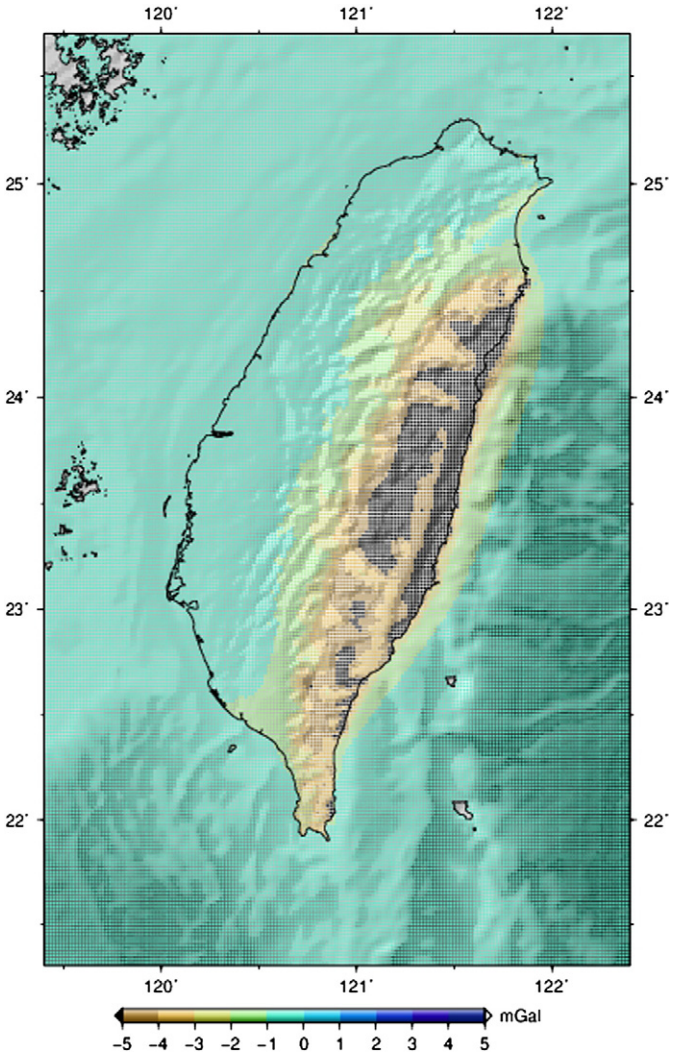

Fig. 5. Differences in BAs due to neglecting oceanic contribution when computing BAs on land, and also neglecting land contribution when computing BAs at sea.

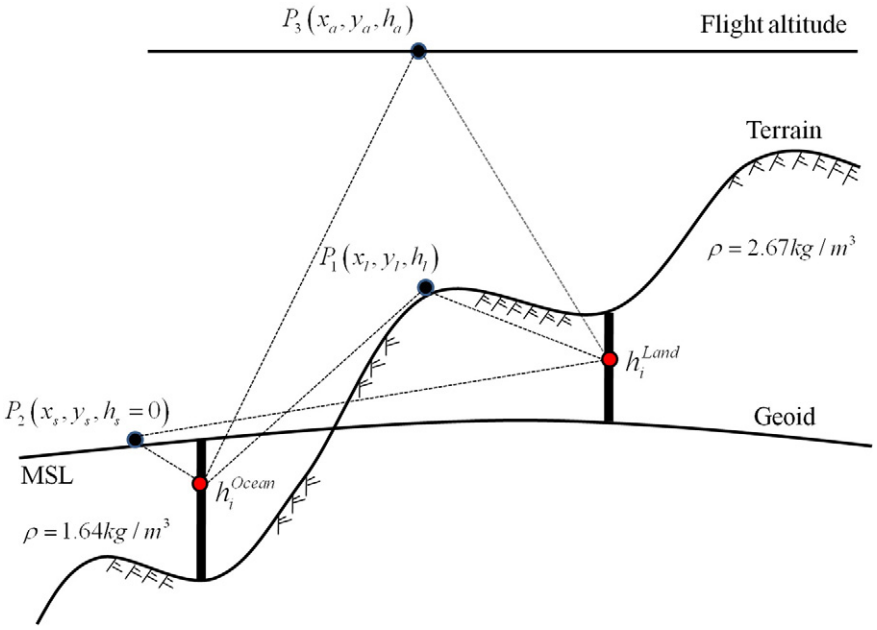

Fig. 4. Geometry showing topographic effect due to land topography and ocean bathymetry.

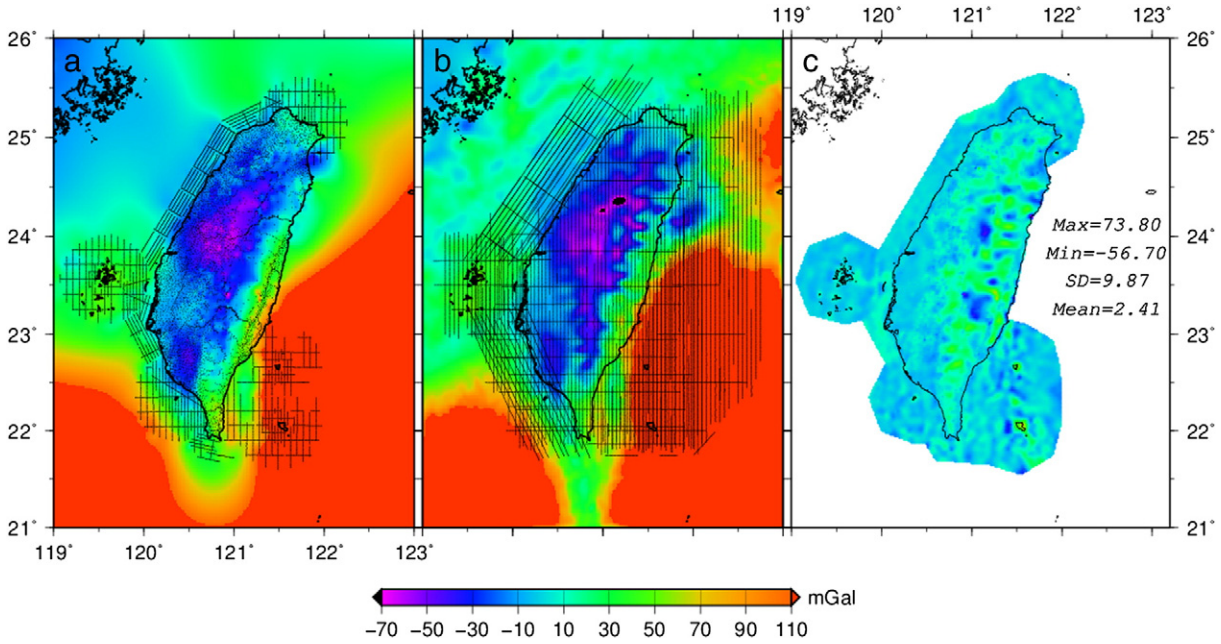

Fig. 6. (a) Bourguer gravity anomalies from land and offshore shipborne campaigns, (b) Bourguer gravity anomalies from airborne gravity campaigns (augmented by altimeter-derived gravity, Section 2.4), (c) differences between the two fields in (a) and (b).

(discussed in Section 3). The downward continuation (for the three airborne gravity datasets) and merging of all BAs onto a $1' \times 1'$ grid were carried out in a one-step procedure using the band-limited least-squares collocation (BL-LSC) (Moritz, 1980):

$$\mathbf{s} = \mathbf{C}_{sg}\left(\mathbf{C}_g + \mathbf{D}_g\right)^{-1}\mathbf{g} \tag{3}$$

with the error covariance matrix of the merged gravity values computed as

$$\mathbf{\Sigma}_S = \mathbf{C}_{ss} - \mathbf{C}_{sg}\left(\mathbf{C}_g + \mathbf{D}_g\right)^{-1}\mathbf{C}_{gs} \tag{4}$$

where $\mathbf{s}$ and $\mathbf{g}$ are vectors containing the merged and raw gravity values, $\mathbf{C}_g$ and $\mathbf{D}_g$ are the covariance matrices of the raw gravity data and their

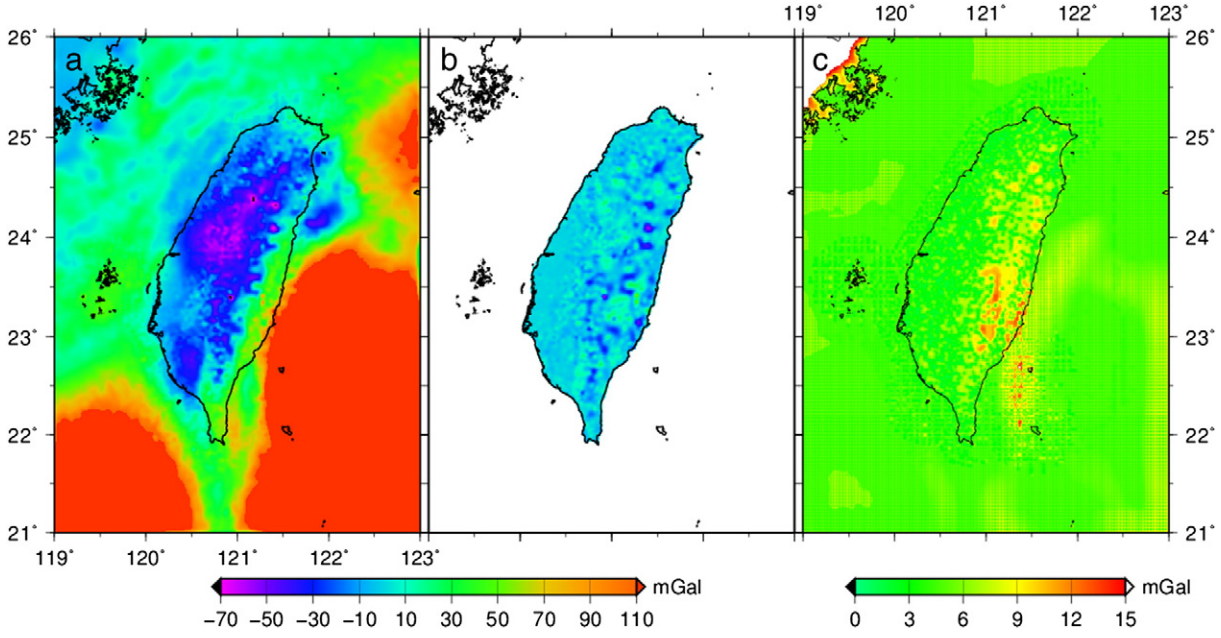

Fig. 7. (a) Bouguer gravity anomalies from all data, (b) differences in BAs between the new field (this paper) and the field from Yen et al. (1990) on land, (c) the standard errors of BAs from LSC.

noises, and $\mathbf{C_{sg}}$ and $\mathbf{C_{gs}}$ are the covariance matrix and its transpose between the merged and the raw gravity anomalies. $\mathbf{D_g}$ is a diagonal matrix containing the error variances of the raw data. The matrix elements of $\mathbf{C_g}$ and $\mathbf{C_{sg}}$ are computed using the general covariance function

$$C_{pq}(\psi) = \sum_{n=2}^{K} \gamma_n \left(\frac{R_B^2}{r_p r_q} \right)^{n+2} P_n(\cos\psi) \quad (5)$$

where r_p and r_q are the geocentric distances to p and q, R_B is the radius of Bjerhammar sphere (Moritz, 1980), P_n is the Legendre polynomial, K is the degree of harmonic expansion associated with the spatial resolution of a given gravity dataset (Table 1) and γ_n is the Model 4 degree variance (Tscherning and Rapp, 1974). The covariance matrices $\mathbf{C_g}$ and $\mathbf{C_{sg}}$ in Eq. (3) are scaled by the ratio between the variance of the residual gravity values in $\mathbf{g}$ and the model variance $\mathbf{C}_{pq}(0)$; see Hwang and Parsons (1995). K corresponds to the half filter window (half-wavelength) of the gravity values collected in a moving platform. The term band-limited is due to the use of K in Eq. (5). There will be different K values for different datasets collected with moving platforms, and K is infinity for the land datasets. For the altimeter-derived gravity, we assume that the corresponding K is infinity because of lack of information about its spatial contents; this assumption will not affect the combined gravity on and near land because the altimeter-derived gravity receives small weights here. According to the coherence analysis of Hwang et al. (2012), the resolving half wavelength of the three airborne sets are listed in Table 1, with the corresponding K values computed as $K =$ 20,000 km/spatial resolution (Hwang et al., 2007).

The factor $R_B^2/(r_p r_q)$ in Eq. (5) introduces the effect of height attenuation in the BL-LSC through the values r_p and r_q. For example, if p (the gravity value at p is stored in vector s) is at sea level and the contributing point value is the 5156-m airborne gravity, we set $r_p = R_e$ and $r_q = R_e + H_q$, where R_e is the radius of the Gaussian mean ellipsoid at the average latitude of Taiwan (24° N) and H_q 5156 m. All the needed covariance function values were pre-computed at a 0.01° interval and the actual values were obtained from interpolation. Because it is

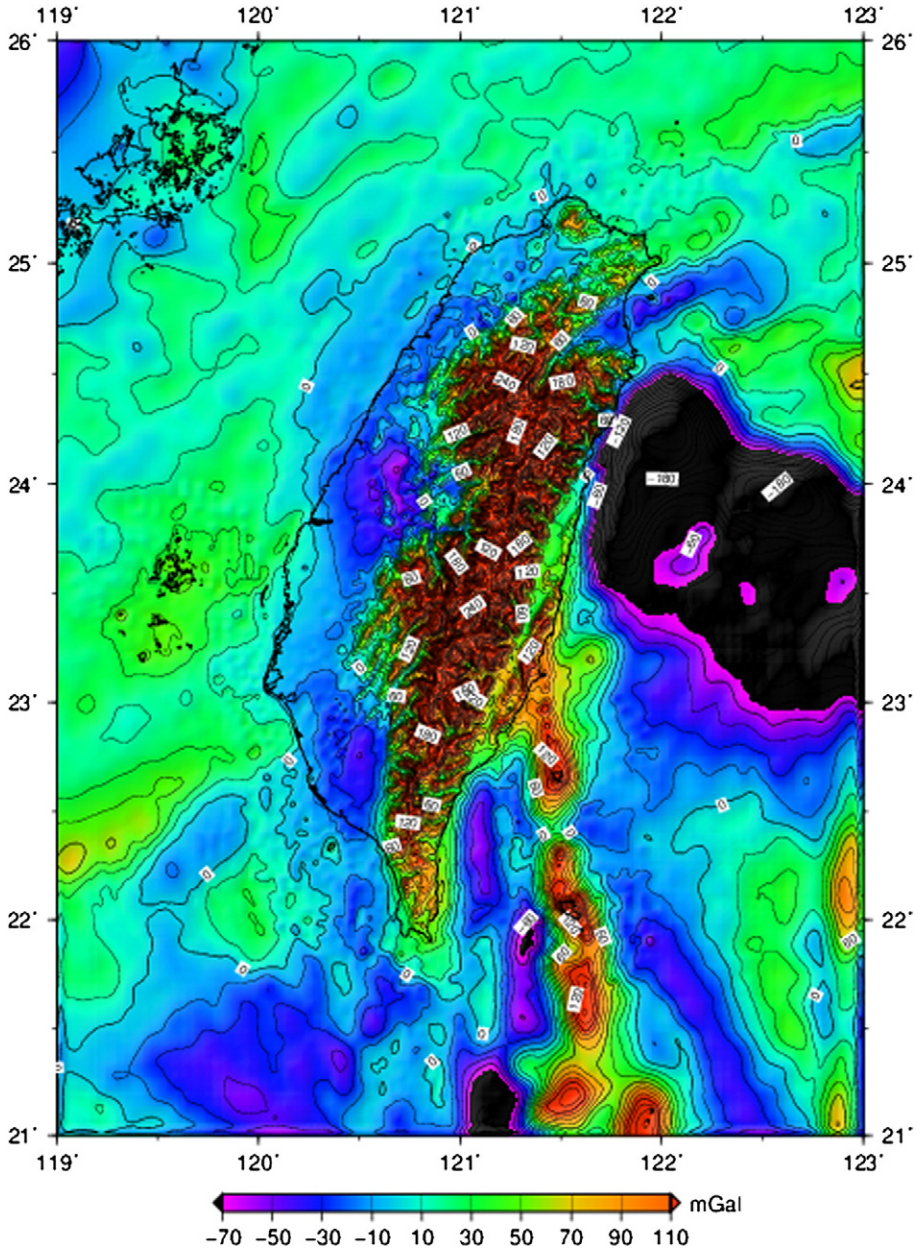

Fig. 8. Free-air gravity anomalies from all data.

difficult to obtain correlation coefficients among point gravity values, the matrices in $\mathbf{D_g}$ in Eq. (4) are assumed to be diagonal with the diagonal elements being the error variances of the raw data (squared standard errors in Table 1, and the squared standard error for NCTU12 in Table 2). To avoid aliasing effects caused by uneven data distributions, the most representative values in $1' \times 1'$ blocks were determined using the means of all values in such blocks. With the sea-level BAs determined, the FAs at ground level were obtained by restoring the contributions of the topography at ground level.

In order to assess the combined BAs, we formed two $1' \times 1'$ grids from ground gravity data only (land and offshore gravity; Fig. 6a) and from the airborne and altimeter-derived gravity data only (Fig. 6b), respectively. The gravity features in Fig. 6a and b closely resemble each other, but with the following notable differences: (1) the airborne BAs are smoother due to the altitude attenuation effect and (2) because the 5156-m gravity lines are evenly distributed over Taiwan, the airborne and altimeter-only BAs fill the data gaps of ground-only gravity and contain gravity signatures missing in the ground-only BAs. In addition, Fig. 6c shows the differences between two fields (land-offshore gravity, Fig. 6a vs. airborne-altimetry gravity, Fig. 6b). The differences range from −56.7 to 73.8 mGal, with the mean and the standard deviation (SD) of 2.41 and 9.87 mGal, respectively. Relatively large differences occur in high mountain areas and around the two islands off the southeast of Taiwan. Figs. 7a and 8 show the combined BA and FA grids. Fig. 7b shows the differences in BAs on land between our new field and the field from Yen et al. (1990). The relatively large differences over high-mountain areas are due to the use of the airborne gravity data and the Mountain-1 gravity data (Table 1). Fig. 7c shows the standard errors of BAs, which are the square roots of the diagonal elements of Σ_s in Eq. (4). The standard errors are quite uniform, but there exist relatively large standard errors over the Central Range and areas off the east coast of Taiwan. The gravity data densities and the gravity field roughness combine to generate the pattern seen in Fig. 7c.

5. Distinct tectonic features from the new Bouguer gravity anomalies

To demonstrate how the new BA field may contribute to resolving high-resolution tectonic features (Fig. 9), in Fig. 10 we show the differences of BAs along 6 selected profiles from the new BA grid and the grid of Yen et al. (1990) across various Taiwan tectonic units. In general, BAs are negatively correlated with the topographic relief in both fields, but the new gravity field gives much higher frequency contents along the profiles. The differences between the new and existing fields are larger over high-elevation zones than the plains. A short summary of the features is given below. Distinct, negative BAs exist over the high-elevation zone of the CeR, revealing the vertical compensation that balances the orogenic mountain loading. An extreme gravity low is centered at about 24°N, 121°E (TP) and is extended to the HR and the northern segment of the western foothill (b–b′ and c–c′). This low has been explained by a huge deposit of the early Tertiary sediments that filled the half-graben caused by the systematic continental margin rifting (the Paleocene syn-rifting and the Neocene–Quaternary post-rifting), typically found at the southeast Eurasia plate (Sun, 1982; Teng, 1992). In addition to the high mountain areas, the Ilan Plain (IP) and Pingtung Plain (PP) in the northeastern and southwestern Taiwan

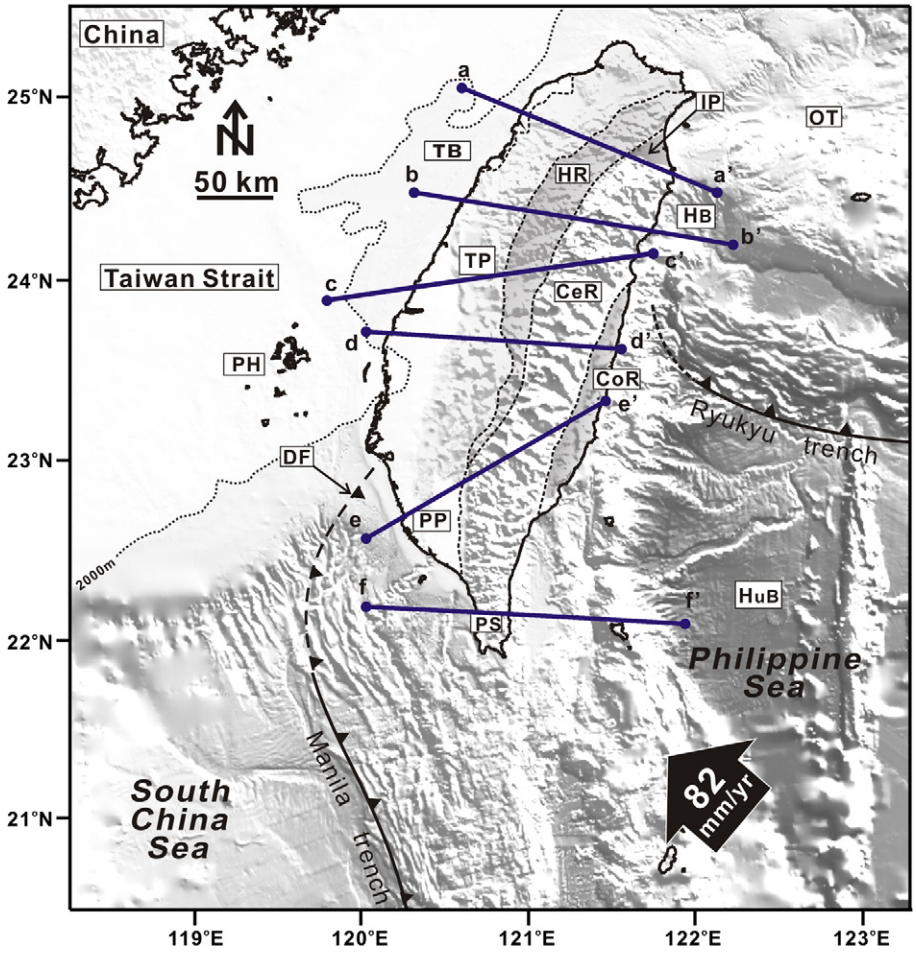

Fig. 9. Locations of 6 profiles with abbreviations of geological features.

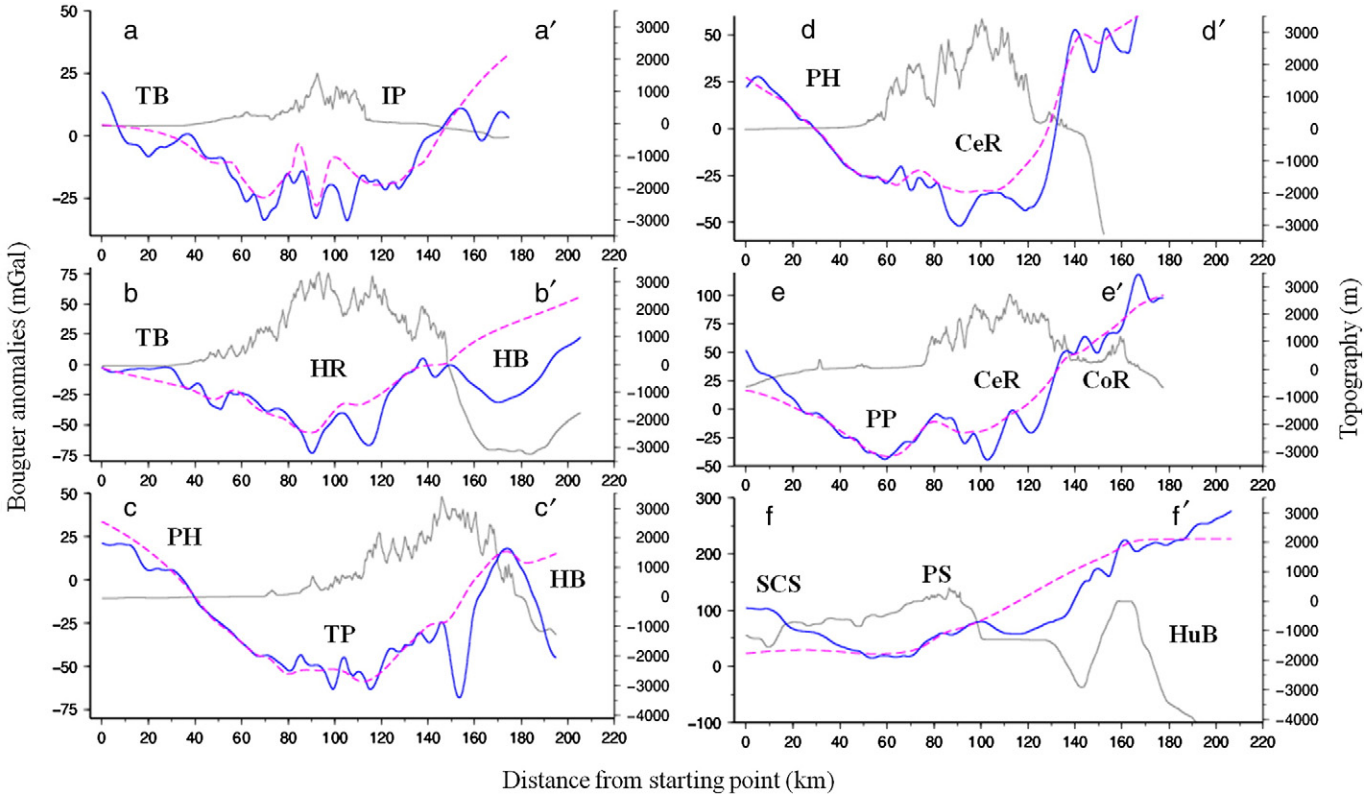

Fig. 10. Along-profile BAs from this paper (blue) and existing data (red) and topography (black). The left and right vertical labels show BA and elevation.

also show Bouguer lows (a–a′ and f–f′). In the Taisi Basin (TB) off the central, western Taiwan and in the Hoping Basin (HB) off the northeastern Taiwan, pronounced Bouguer lows also exist. Findings and interpretations of these gravity features have been presented before, but our new BA field will significantly revise earlier results, especially for interpretations extending to offshore areas of Taiwan. Over the Okinawa Trough (OT), the BAs decrease westwards, turning to negative values off the IP. This suggests that IP is a result of sedimentary deposits, instead of a high-density magma chamber associated with the back-arc spreading east of the IP (e.g. Ho, 1986). Over the Huatung Basin (HuB), again the BAs are positive and decrease towards the CoR, becoming negative along a belt west of the LV. Such a narrow transition zone from the oceanic crusts to the Eurasia crust around Taiwan will inspire further investigations. More applications of the BA field are left to interested readers.

6. Conclusions

We construct a high resolution and coherent gravity field from multiple gravity datasets. The new BA and FA grids show a wealth of gravity signatures not seen in previous maps of Taiwan gravity. The edited gravity datasets will offer new insights for geophysical and geodetic studies, particularly for issues covering both land and sea, and both continental crust and oceanic crust. They can be used to test various hypotheses of geodynamic processes and geodetic theories. One notable advantage our new datasets is to see different gravity signatures from a common source at different altitudes. Such altitude-varying gravity datasets will help to constrain the inversion of the source and can be used to assess downward continuation theories. There are several first-order leveling routes with sub-cm vertical height accuracy from GPS (Chu and Yang, 2013) to assess any potential methods of geoid modeling and vertical datum connection. Because the geodetic positions of the gravity stations were determined to cm–dm levels and we used a latest DEM of Taiwan, the FAs and BAs are determined with unprecedented accuracies. In order not to underestimate BAs, we should consider both land and oceanic mass contributions, as demonstrated in Section 3.

For the first time, offshore gravity data with few tens of m to coastlines were collected on small vessels around Taiwan, yielding gravity data with much smaller standard errors (at few mGal level) than those collected in large research vessels (at tens of mGal in some cases). Such nearshore gravity values will be valuable for enhancing gravity interpretations of geodynamic features near coasts, and for assessing offshore altimeter-derived gravity fields from the latest satellite missions such as Jason-1/GM and Cryosat-2.

Acknowledgments

The projects to collect the gravity data are supported by the National Land Survey and Mapping Center, and the Ministry of the Interior, Taiwan. The manpower to compile the data is supported by the National Science Council of Taiwan, under grants 100-2221-E-009-132-MY3 and 101-2611-M-009-001.

References

Amante, C., Eakins, B.W., 2009. ETOPO1 1 arc-minute global relief model: procedures, data sources and analysis. NOAA Technical Memorandum NESDIS NGDC-24, p. 19.
Andersen, O.B., 2010. The DTU10 gravity field and mean sea surface. Second International Symposium of the Gravity Field of the Earth (IGFS), Fairbanks, Alaska.
Chang, S.S.L., Hu, C.C., 1981. Gravity and magnetic anomalies of Taiwan and their tectonic implication. Mem. Geol. Soc. China 4, 121–142.
Chu, F.Y., Yang, M., 2013. GPS/Galileo long baseline computation: method and performance analyses. GPS Solutions. http://dx.doi.org/10.1007/s10291-013-0327-7.

Featherstone, W.E., 2013. Deterministic, stochastic, hybrid and band-limited modifications of Hotine's integral. J. Geod. 87 (5), 487–500. http://dx.doi.org/10.1007/s00190-013-0612-9.
Ho, C.S., 1986. A synthesis of the geologic evolution of Taiwan. Tectonophysics 125, 1–16. http://dx.doi.org/10.1016/0040-1951(86)90004-1.
Hsieh, S.H., Hu, C.C., 1972. Gravimetric and magnetic studies of Taiwan. Pet. Geol. Taiwan 10, 283–321.
Hsieh, H.H., Yen, H.Y., Shih, M.H., 2010. Moho depth derived from gravity data in the Taiwan Strait area. Terr. Atmos. Ocean. Sci. 21, 235–241. http://dx.doi.org/10.3319/TAO.2009.03.05.01(T).
Hsu, S.K., Liu, C.S., Shyu, C.T., Liu, S.Y., Sibuet, J.C., Lallemand, S., Wang, C., Reed, D., 1998. New gravity and magnetic anomaly maps in the Taiwan–Luzon region and their preliminary interpretation. Terr. Atmos. Ocean. Sci. 9, 509–532.
Huang, T.Y., Gung, Y., Liang, W.T., Chiao, L.Y., Teng, L.S., 2012. Broad-band Rayleigh wave tomography of Taiwan and its implications on gravity anomalies. Geophys. Res. Lett. 39, L05305. http://dx.doi.org/10.1029/2011GL050727.
Hwang, C., 1998. Inverse Vening Meinesz formula and deflection-geoid formula: applications to the predictions of gravity and geoid over the South China Sea. J. Geod. 72 (5), 304–312. http://dx.doi.org/10.1007/s001900050169.
Hwang, C., Kao, R., 2002. TOPEX/POSEIDON-derived space–time variations of the Kuroshio Current: applications of a gravimetric geoid and wavelet analysis. Geophys. J. Int. 151 (3), 835–847. http://dx.doi.org/10.1046/j.1365-246X. 2002.01811.x.
Hwang, C., Parsons, B., 1995. Gravity anomalies derived from Seasat, Geosat, ERS-1 and TOPEX/POSEIDON altimetry and ship gravity: a case study over the Reykjanes Ridge. Geophys. J. Int. 122, 551–568. http://dx.doi.org/10.1111/j.1365-246X.1995.tb07013.x.
Hwang, C., Wang, C.G., Lee, L.H., 2002. Adjustment of relative gravity measurements using weighted and datum-free constraints. Comput. Geosci 28 (9), 1005–1015. http://dx.doi.org/10.1016/S0098-3004(02)00005-5.
Hwang, C., Hsiao, Y.S., Lin, T.L., 2003. A digital elevation model of Taiwan and accuracy assessment. Cadastre Surv. 22, 1–19 (in Chinese).
Hwang, C., Hsiao, Y.S., Shih, H.C., Yang, M., Chen, K.H., Forsberg, R., Olesen, A.V., 2007. Geodetic and geophysical results from a Taiwan airborne gravity survey: data reduction and accuracy assessment. J. Geophys. Res. Solid Earth 112, B04407. http://dx.doi.org/10.1029/2005JB004220.
Hwang, C., Shih, H.C., Hsiao, Y.S., Huang, C.H., 2012. Airborne gravity surveys over Taiwan Island and Strait, Kuroshio Current and South China Sea: comparison of GPS and gravity accuracies at different flight altitudes. Mar. Geod. 35 (3), 287–305. http://dx.doi.org/10.1080/014904192011.634962.
Hwang, C., Hsu, H.J., Huang, C.H., 2013. A new geoid model of Taiwan: applications to hazard mitigation, environmental monitoring and height modernization. Taiwan J. Geoinform. 1 (1), 57–81 (in Chinese).
Kirby, J.F., 2003. On the combination of gravity anomalies and gravity disturbances for geoid determination in Western Australia. J. Geod. 77 (7–8), 433–439. http://dx.doi.org/10.1007/s00190-003-0334-5.
Kuo-Chen, H., Wu, F., Roecker, S., 2012. Three-dimensional P velocity structures of the lithosphere beneath Taiwan from the analysis of TAIGER and related seismic datasets. J. Geophys. Res. 117 (B6). http://dx.doi.org/10.1029/2011JB009108.
Lin, A.T., Watts, A.B., 2002. Origin of the West Taiwan basin by orogenic loading and flexure of a rifted continental margin. J. Geophys. Res. 107 (B9), 2185. http://dx.doi.org/10.1029/2001JB000669.
Masson, F., Mouyen, M., Hwang, C., Wu, Y.M., Ponton, F., Lehujeur, M., Dorbath, C., 2012. Lithospheric structure of Taiwan from gravity modelling and sequential inversion of seismological and gravity data. Tectonophysics 578, 3–9. http://dx.doi.org/10.1016/j.tecto2012.04.012.
Moritz, H., 1980. Advanced Physical Geodesy. Abacus Press, Tunbridge Wells.
Novák, P., Heck, B., 2002. Downward continuation and geoid determination based on band-limited airborne gravity data. J. Geod. 76 (5), 269–278. http://dx.doi.org/10.1007/s00190-002-0252-y.
Pavlis, N.K., Holmes, S.A., Kenyon, S.C., Factor, J.K., 2013. Correction to "The development and evaluation of the Earth Gravitational Model 2008 (EGM2008)". J. Geophys. Res. Solid Earth. http://dx.doi.org/10.1029/jgrb.50167.
Pope, A.J., 1976. The statistics of residuals and the detection of outliers. Technical Report S65. US National Geodetic Survey, Rockville, Maryland, USA, p. 133 (http://www.ngs.noaa.gov/PUBS_LIB/TRNOS65NGS1.pdf).
Sandwell, D.T., Smith, W.H.F., 2009. Global marine gravity from retracked Geosat and ERS-1 altimetry: ridge segmentation versus spreading rate. J. Geophys. Res. Solid Earth 114, B01411. http://dx.doi.org/10.1029/2008JB006008.
Sproule, D.M., Featherstone, W.E., Kirby, J.F., 2006. Localised gross-error detection in the Australian land gravity database. Explor. Geophys. 37 (2), 175–179. http://dx.doi.org/10.1071/EG06175.
Sun, S.C., 1982. The Tertiary basins of offshore Taiwan. In: Salivar-Sali, A. (Ed.), Proceedings of the Second ASCOPE Conference and Exhibition, pp. 125–135 (Manila, Philippines).
Teng, L.S., 1992. Geotectonic evolution of Tertiary continental margin basins of Taiwan. Pet. Geol. Taiwan 27, 1–19.
Tenzer, R., Hamayun, K., Vajda, P., 2009. Global maps of the CRUST 2.0 crustal components stripped gravity disturbances. J. Geophys. Res. Solid Earth 114, B05408. http://dx.doi.org/10.1029/2008JB006016.
Torge, W., 1989. Gravimetry. deGruyter, Berlin.
Tscherning, C.C., Rapp, R.H., 1974. Closed covariance expressions for gravity anomalies, geoid undulations and deflections of the vertical implied by anomaly degree variance models. Rep. No. 208, Dept. of Geod. Sci. and Surv. The Ohio State Univ, Columbus, Ohio.
Wessel, P., Smith, W.H.F., 1998. New, improved version of Generic Mapping Tools released. EOS Trans. Am. Geophys. Union 79 (47), 579.
Yang, M., Tseng, C.L., Yu, J.Y., 2001. Establishment and maintenance of Taiwan geodetic datum 1997. J. Surv. Eng. 127 (4), 119–132.
Yang, Y., Hwang, C., Hsu, H.J.E.D., Wang, H., 2011. A subwaveform threshold retracker for ERS-1 altimetry: a case study in the Antarctic Ocean. Comput. Geosci. 41 (1), 88–98. http://dx.doi.org/10.1016/j.cageo.2011.08.017.
Yen, H.Y., Yeh, Y.H., Lin, C., 1990. Free-air gravity maps of Taiwan and its applications. Terr. Atmos. Ocean. Sci. 1 (2), 143–155.